Investigation of Chromatic Dispersion Properties of Athermal 100 GHz Cyclic AWG for Super PON

2025 17th International Conference on Advanced Infocomm Technology (ICAIT) | 979-8-3315-7912-8/25/$31.00 ©2025 IEEE | DOI: 10.1109/ICAIT66450.2025.11353294

Jozef Chovan*
International Laser Centre
Slovak Centre of Scientific and Technical Information
Bratislava, Slovakia
jozef.chovan@cvtisr.sk
*Corresponding author

Ignác Bugár
International Laser Centre
Slovak Centre of Scientific and Technical Information
Bratislava, Slovakia
ignac.bugar@cvtisr.sk

Anton Kuzma
International Laser Centre
Slovak Centre of Scientific and Technical Information
Bratislava, Slovakia
anton.kuzma@cvtisr.sk

Martin Tomaška
International Laser Centre
Slovak Centre of Scientific and Technical Information
Bratislava, Slovakia
martin.tomaska@cvtisr.sk

***Abstract*—This paper presents a simulation-based investigation of the dispersion characteristics of a 20-channel, 100 GHz cyclic arrayed waveguide grating (CAWG) with a 2.2 THz free spectral range, evaluated across four free spectral range bands within the C and L telecommunications bands for Super PON applications. The CAWG is designed using an athermal waveguide structure comprising a silicon oxynitride (SiOxNy) core layer, a polymethyl methacrylate (PMMA) cladding layer, and a silicon substrate with a thermally grown silicon dioxide buffer layer. This configuration effectively mitigates temperature-induced shifts in the central wavelength. In addition to the athermal design, this work introduces a novel analysis of both waveguide and material dispersion effects in the cyclic AWG structure. The dispersion behavior is evaluated across four spectral periods, providing a comprehensive understanding of the transmission characteristics and spectral alignment of the CAWG under varying conditions. The device with central wavelength 1555.35 nm, is modeled using the Synopsys BeamPROP AWG utility. The results offer new insights into the interplay between thermal stability and chromatic dispersion in cyclic AWG devices for next-generation optical access networks.**

Keywords— athermal waveguide, SiON, cyclic AWG, super PON, chromatic dispersion, PMMA

I. INTRODUCTION

An arrayed waveguide grating (AWG) can be seamlessly integrated into photonic integrated circuits (PICs), offering significant advantages over conventional filtering techniques in telecommunications applications. Fig. 1 illustrates the basic topology of an AWG structure. AWG is a planar waveguide structure consisting of two symmetrical couplers connected with each other by an array of waveguides (called phased array, PA) and I/O waveguides [1]. However, the performance of traditional AWGs is highly sensitive to temperature fluctuations, which can lead to a shift in the central wavelength, denoted as λ_c (Fig. 2), and increased insertion losses. This temperature dependence poses a major challenge for deploying AWG-based photonic circuits in outdoor environments where thermal stabilization via active control is not feasible. To address this issue, athermal AWG designs have been proposed, where the temperature insensitivity is achieved by incorporating athermal waveguides within the phased array (PA) section of the AWG (Fig. 1). In this context, the combination of silicon oxynitride (SiOxNy) as the core waveguide material and polymethylmethacrylate (PMMA) as the cladding layer presents a promising solution. SiOxNy exhibits a low positive thermo-optic coefficient, while PMMA offers a high negative thermo-optic coefficient along with excellent optical properties. Together, these materials enable effective compensation of thermal effects, thereby stabilizing the AWG's spectral response. Furthermore, integrating these materials on a silicon substrate with a thermal silicon dioxide (SiO_2) buffer layer leverages the maturity of the silicon photonics platform and ensures compatibility with standard fabrication processes. This integration supports the development of compact, cost-effective, and high-performance photonic devices suitable for large-scale deployment [1]. The primary motivation of this research is to design an athermal 20 channels 100GHz cyclic AWG tailored for Super-PON (IEEE 802.3cs-2022), capable of operating efficiently across a wide temperature range from -40 °C to 80 °C without active thermal control. By utilizing SiOxNy and PMMA on a silicon substrate with a thermal SiO_2 buffer, we aim to

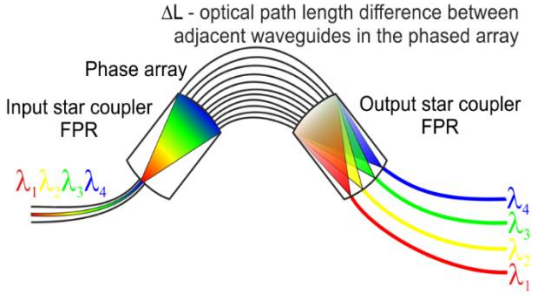


Fig. 1. Basic topology of AWG [1].

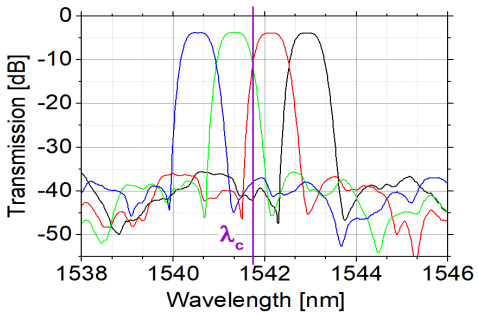


Fig. 2. AWG transmission characteristics consisting of four channels with the AWG central wavelength, lc illustration [1].

This work was funded by the EU NextGenerationEU through the Recovery and Resilience Plan for Slovakia under the project No. 09I03-03-V04-00684

Authorized licensed use limited to: CVTI - Centre of Scientific and Technical Info. Downloaded on July 21,2026 at 08:11:17 UTC from IEEE Xplore. Restrictions apply.

significantly reduce the temperature-induced shift in the central wavelength λ_c, thereby enhancing the performance and reliability of Super-PON systems based on cyclic AWG wavelength routers [2]. Super PON represents a next-generation passive optical network (PON) architecture, supporting extended optical reach up to 50 km and accommodating up to 1024 users per feeder fiber. This is achieved through the integration of wavelength division multiplexing (WDM), optical amplification, wavelength routing, and existing time division multiplexing (TDM) PON protocols [3]. CAWG acts in super PON as wavelength router with four bands of its output channels over spectral band more than 70 nm over C and L telecon band. The impact of chromatic dispersion on the CAWG central wavelengths of each band of athermal CAWG output channels based on athermal waveguide [2] is analyzed through numerical simulations. Previous studies [4-6] have primarily focused on the design and thermal stability of AWG central wavelength shift this spectral range only few units' nm [6], often neglecting detailed chromatic dispersion analysis, especially in cyclic designs. In contrast, our work provides a combined investigation of waveguide and material dispersion in a cyclic AWG device over more than 70 nm spectrum range. This dual-layered analysis across multiple spectral periods offers deeper insight into the performance and potential application of such devices in WDM-TDM PON architectures.

II. Athermal Waveguide Structure

The contour map of the transverse refractive index profile of used athermal rib waveguide structure is shown in Fig. 3 [2]. The use of SiOxNy as the core material (depicted in red) and polymethylmethacrylate (PMMA) as the cladding layer (shown in blue) plays a crucial role in achieving the desired athermal behavior on a silicon substrate with a thermal SiO_2 buffer layer. The refractive index of the SiOxNy layer can be tailored during deposition via plasma-enhanced chemical vapor deposition (PECVD), with achievable values ranging from 1.447 to 1.651 at a wavelength of λ = 1.55 µm [7]. This tunability allows precise control over the refractive index contrast between the SiOxNy core and the PMMA cladding, directly influencing the temperature dependence of the waveguide's effective refractive index. The thermo-optic coefficient (TOC) of the SiOxNy layer exhibits a linear dependence from 10×10^{-6} °C^{-1} to 16×10^{-6} °C^{-1} on its refractive index from 1.44 to 1.66 [8]. PMMA, with a refractive index of approximately 1.480 at 1550 nm and a negative TOC of - 170×10^{-6} °C^{-1}, contributes significantly to the athermal design [9]. This negative TOC enables compensation for the positive TOC of the SiOxNy core, allowing the effective refractive index to exhibit a negative temperature dependence. PMMA is a flexible, optically transparent polymer that is compatible with standard photolithographic processes, making it ideal for integration into photonic structures. Its low optical absorption in the visible and near-infrared regions ensures minimal insertion loss, further enhancing the performance of the waveguide. Figure 4 shows vertical cut of refractive index changes at X = 0 µm position of athermal waveguide structure for 60°C positive and 40°C negative temperature changes. The Y-axis in Figure 4 corresponds to the designation in Figure 3. The change in the refractive index of the PMMA layer is several times greater than the change in the refractive index of SiOxNy and thermal SiO_2 according to TOC values. The material dispersions of the waveguide materials in spectral band from 420 nm to 2 000 nm are shown in Fig. 5 [7-9]. In the telecommunication bands C and L, there is a consistent decrease in the refractive index values of all layers with increasing wavelength. The effective refractive index of the athermal waveguide structure was calculated by beam probe methods including thermo-optical effect of each waveguide structure layers and materials and waveguide dispersion for three temperatures –40°C, –20°C and 80°C at 1525 nm – 1610 nm spectral band. The dependence of the effective refractive indices of the athermal waveguide on the wavelength for the investigated spectral region for three different temperatures - 40°C, 20°C and 80°C are shown in Fig. 6. The absolute maximum variation in the effective refractive index of the athermal waveguide, resulting from a temperature change of 120 °C across the entire investigated spectral range (1525 nm to 1610 nm), was found to be less than 0.7 e-3. The absolute maximum change in the effective refractive index of an athermal waveguide due to material and waveguide dispersion is at the level of 2.6 e-3, which is more than three times larger than the change caused by a temperature change of 120°C. From this fact, it can be assumed that the dominant influence on the chromatic dispersion of the CAWG transmission properties in the spectral range of four bands of the output channels will be the material and waveguide dispersion

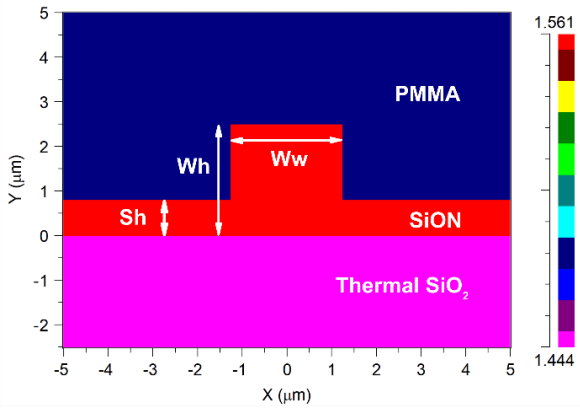


Fig. 3. Contour map of transverse refractive index profile of used athermal waveguide structure.

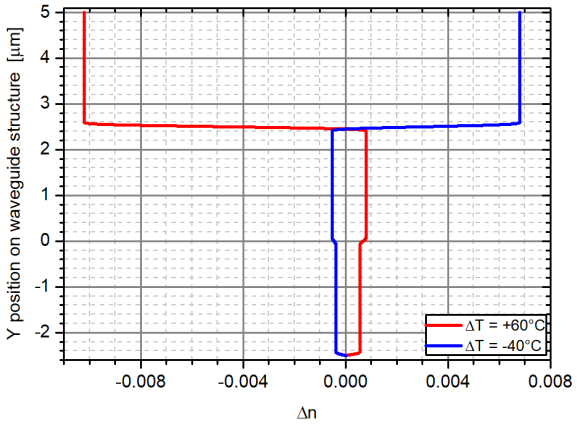


Fig. 4. Vertical cut of refractive index changes at X = 0 mm position of designed athermal waveguide structure.

Authorized licensed use limited to: CVTI - Centre of Scientific and Technical Info. Downloaded on July 21,2026 at 08:11:17 UTC from IEEE Xplore. Restrictions apply.

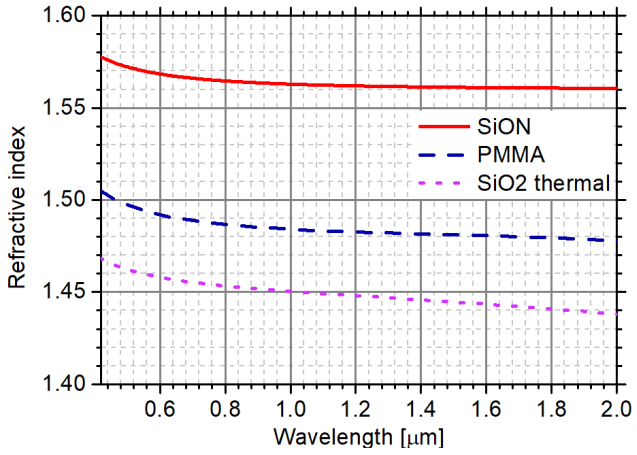


Fig. 5. Material dispersion of athermal waveguide structure materials.

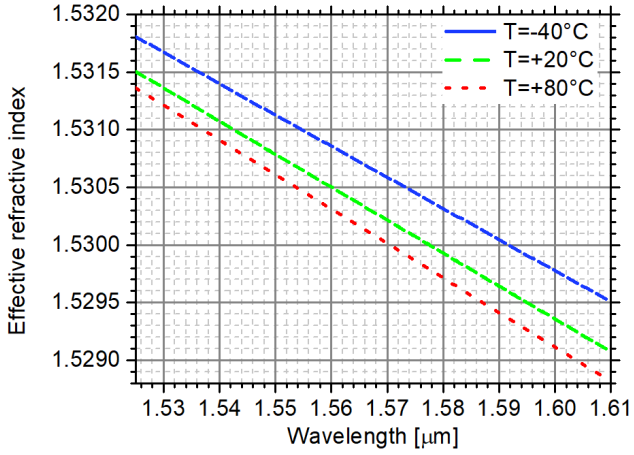


Fig. 6. Effective refractive index of the athermal waveguide structure materials, incorporating both material and waveguide dispersion effects.

and not the influence of temperature changes. Even though the TOC values of individual waveguide layers are constant, with a negative temperature change of 60°C, the change in the effective refractive index of the athermal waveguide is greater than with a positive temperature change of 60°C. This higher change in the effective refractive index for a negative temperature change is caused by waveguide dispersion, due to the change in the refractive index contrast between the SiON and PMMA layers. With a negative temperature change, the refractive index of the PMMA layer increases and the refractive index of the SiON decreases, thereby decreasing the refractive index contrast at the interface of these two layers of the athermal waveguide, which affects the waveguide effect and causes waveguide dispersion.

III. Design and Simulation of Athermal CAWG

The 20-channel, 100-GHz athermal CAWG with 2.2 THz FSR was designed for central wavelength of λ_c = 1 555.35 nm. The designed CAWG topology parameters were calculated by Synopsys BeamPROP AWG Layout Utility. Input parameters of this AWG Layout Utility are number of input and output ports, spectral channel spacing, central wavelength, FSR and waveguide structure. We used our athermal waveguide structure published in [2]. Fig. 7 shows the layout of the designed cyclic AWG, created using the AWG Layout Utility. To generate the CAWG layout, we used a minimum waveguide bend radius of 900um, to minimize bending losses [2]. The design area of the CAWG on the photonic chip is less than 36 mm². Fig. 8 displays four bands of the simulated transmission characteristics of the CAWG with a 2.2 THz FSR, which are utilized in the Super PON system [3] over C and L telecom bands. In the following parts of this article, we use the designation of individual bands of the transmission spectral characteristics of the simulated and investigated CAWG C2, C1, L2 and L1 from left to right in the spectral region. In the simulation of the transmission characteristics of the CAWG, we considered the material and waveguide dispersion of used athermal waveguide for three different temperatures in the total temperature range of 120°C (Fig.6). Fig. 9 presents the simulated transmission characteristics at the C1 band of the CAWG, obtained using the Synopsys BeamPROP AWG Utility. C1 is the fundamental band for which the CAWG is designed with a central wavelength of 1555.35 nm. The central wavelength of CAWG is the middle spectral position between two central output channels 10th and 11th at band C1 and fits very well with the desired value. Maximum transmission values for all outputs of the designed CAWG are from -1dB to -4dB. Fig. 10 shows the simulated output transmission characteristics of the two central channels

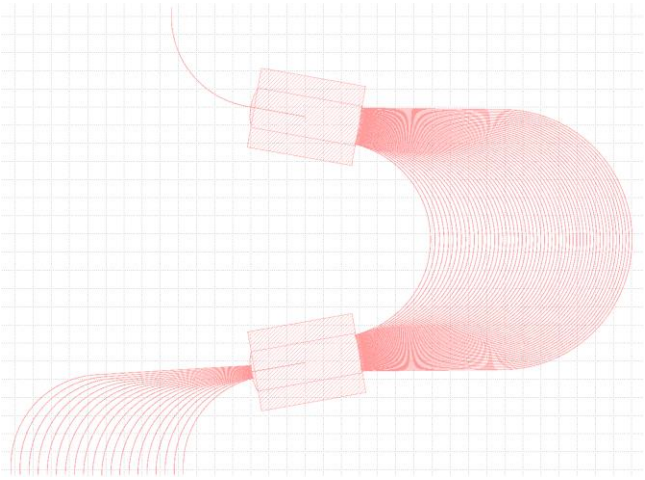


Fig. 7. AWG layout designed by Synopsysy AWG Utility.

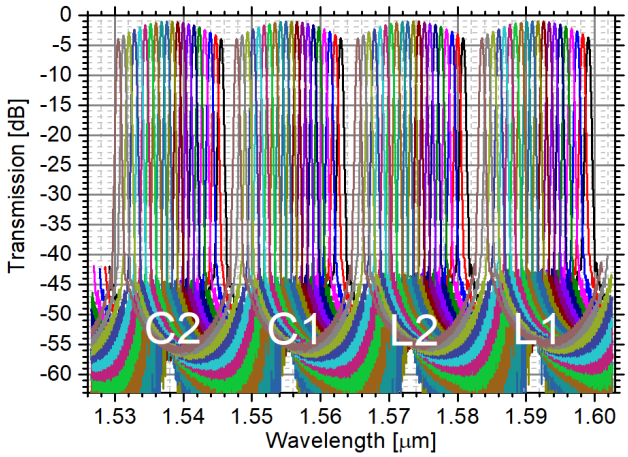


Fig. 8. Simulated transmission characteristics of four CAWG bands.

Authorized licensed use limited to: CVTI - Centre of Scientific and Technical Info. Downloaded on July 21,2026 at 08:11:17 UTC from IEEE Xplore. Restrictions apply.

10th and 11th of CAWG at each band a) C2; b) C1; c) L2 and d) L1 for three different temperatures to illustrate the effect of temperature on CW shift in each investigated band of CAWG for super PON. The smallest effect of temperature on the CW shift of CAWG is in the C1 band, because an athermal waveguide [2] was designed and optimized for this band. In other CAWG bands for super PON, the effect of temperature on CW is more visible. The further the band is from the C1

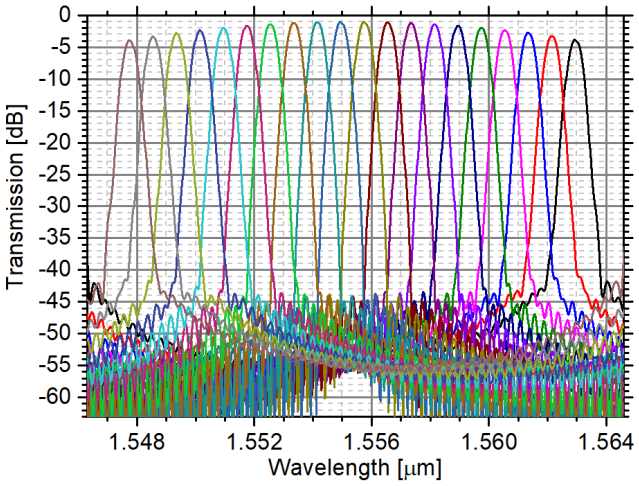
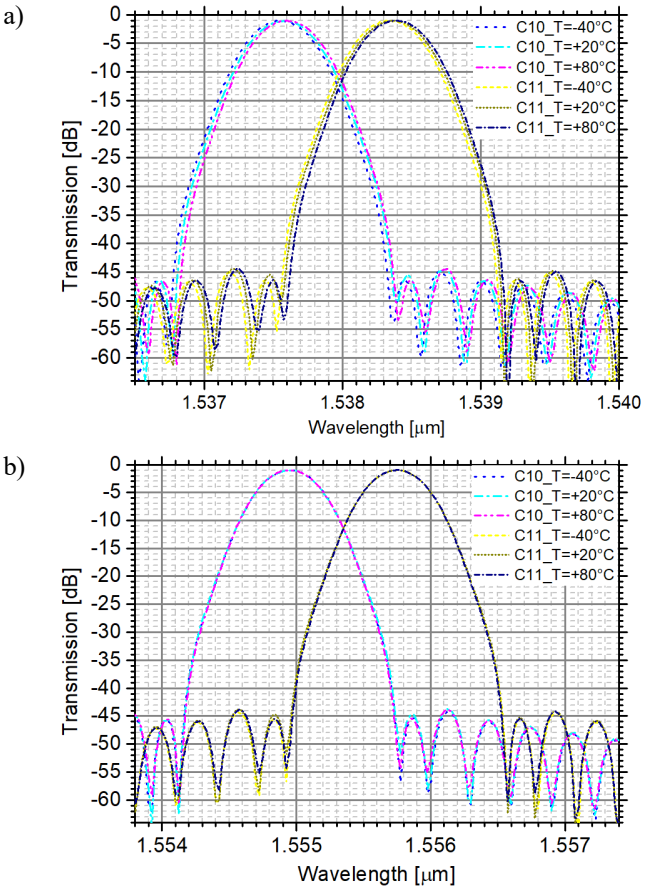


Fig. 9. Simulated output transmission characteristics of CAWG at the C1 band.



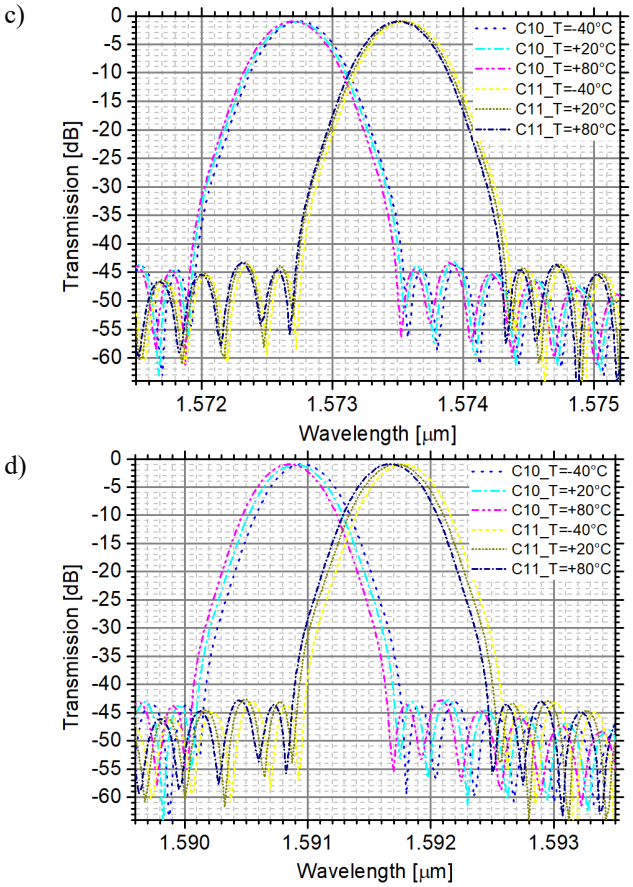


Fig. 10. Simulated output transmission characteristics of the two central channels 10th and 11th of CAWG at each band a) C2; b) C1; c) L2 and d) L1 for three different temperature.

baseband, the greater the effect of temperature change on CW shift. In the C2 band, whose CW is at a shorter wavelength than the C1 base band, it shifts to the right in the spectrum with increasing temperature and to the left with decreasing temperature. In the L2 and L1 bands, whose CWs are at longer wavelengths than the CW of the base C1 band, the effect of temperature on the CW shift is opposite to that for the C2 band. The greatest effect of temperature on the CW shift is in the L1 band, whose CW is furthest from the CAWG baseband CW. To determine the absolute CW shifts for the three considered temperatures, we automatically evaluated the CW, by lab made python code, as the average of the wavelength where transmission has dropped 3 dB from the peak transmission for all 20 CAWG channels in all four super PON bands. The spectral resolution of the output transmission characteristics simulation is 32 points per channel, which is a value of 25pm. This value determines the accuracy of the calculation of the CW values of the CAWG output channels. In Fig. 11, the CW offset of all 20 CAWG channels with ITU DWDM frequency grid [10] is evaluated for the three considered temperatures in all four super PON bands. As was already evident from Fig. 10, the smallest differences in offsets compared to the ITU grid are in the C1 band and the largest are in the L1 band due to the chromatic dispersion of the used athermal waveguide optimized for the 1550 nm wavelength. Tab. 1 evaluates the minimum and maximum CW offsets

Authorized licensed use limited to: CVTI - Centre of Scientific and Technical Info. Downloaded on July 21,2026 at 08:11:17 UTC from IEEE Xplore. Restrictions apply.

of individual CAWG channels relative to the ITU grid in each super PON bands and their differences. The large differences achieved are dominantly caused by the waveguide dispersion of the used athermal waveguide [2]. These large differences compared to the ITU grid indicate the need for further optimization of the athermal waveguide used to reduce its spectral dispersion. The evaluated offset differences in individual super PON bands relative to the ITU grid in Tab. I include the influence of temperature and chromatic dispersion of used athermal waveguide. To separate the effect of temperature and waveguide chromatic dispersion on the offset of the CW output channels of the CAWG relative to the ITU grid, we evaluated the CW shift due to a temperature change of +- 60°C relative to the CW of individual channels at a nominal temperature of 20°C for all four super PON bands. In Fig. 12, there are discrete points that represent the evaluated offsets in the CAWG output channels in individual bands for temperature changes from 20°C to -40°C and from 20°C to 80°C. The achieved CW offsets due to temperature are comparable to the 25 pm spectral resolution of the simulation. For this reason, we also evaluated the average offsets of all 20 CAWG channels for two values of temperature change of +-60°C from the nominal 20°C. The solid lines in Fig. 12 represent the average offset values for each band at each temperature change from nominal. In Tab. II the exact values of the maximum and minimum offsets of CW versus CW and their differences in each super PON bands are given. In Tab. II, the normalized CW shift per 1°C (CWS) from the values of the channels with the largest offsets and from the average offsets of all 20 CAWG channels (Avg CWS) are also evaluated. Tab. III quantitatively calculates the CW shift values caused

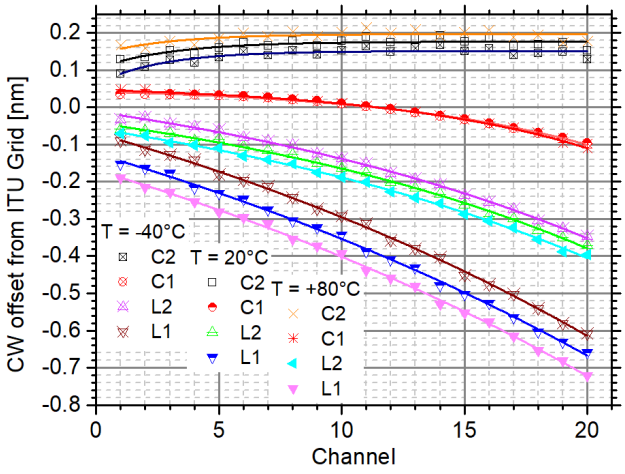


Fig. 11. CW offset from ITU GRID for all four investigated bands of the output transmission characteristics of 20 CAWG outputs.

TABLE I. CW OFFSETS FROM ITU GRID

CW offsets from ITU grid	Bands			
	C2	*C1*	*L2*	*L1*
Max [nm]	0.214	0.048	-0.026	-0.090
Min [nm]	0.091	-0.110	-0.396	-0.721
Overall [nm]	**0.123**	**0.157**	**0.370**	**0.632**

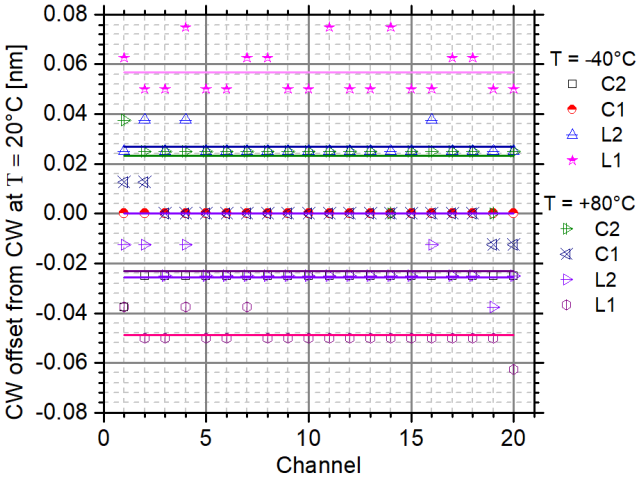


Fig. 12. CW offset from CW at nominal 20°C at two different teperature - 40°C and 80°C for all four super PON bands.

TABLE II. CW OFFSETS FROM CW AT NOMILNAL 20°C

CW offsets from CW at 20°C	Bands			
	C2	*C1*	*L2*	*L1*
Max [nm]	0.037	0.012	0.038	0.075
Min [nm]	-0.038	-0.012	-0.038	-0.063
Overall [nm]	0.075	0.024	0.076	0.138
CWS [pm/°C]	0.625	0.200	0.633	1.150
Avg Max [nm]	0.023	0	0.026	0.057
Avg Min [nm]	-0.026	0	-0.023	-0.049
Avg Overall [nm]	**0.049**	**0**	**0.049**	**0.106**
Avg CWS [pm/°C]	0.408	0	0.408	0.883

TABLE III. EFFECT OF TEMPERATURE AND CHROMATIC DISPERSION ON CW OFFSET

CW offsets from ITU grid	Bands			
	C2	*C1*	*L2*	*L1*
Overall [nm]	0.123	0.157	0.370	0.632
Caused by temperature [nm]	0.049	0	0.049	0.106
Caused by chromatic dispersion [nm]	0.074	0.157	0.321	0.526

by the influence of a temperature change of 120°C and the chromatic dispersion of the waveguide in all four super PON bands. Table III is based on Tables I and II from the lines in bold font. In the C2 band, the effect of temperature and chromatic dispersion of the waveguide is comparable to the CW offset from the ITU grid. In the other three super PON bands C1, L2 and L1, the influence of chromatic dispersion on the CW shift from the ITU grid is dominant. To reduce the CWS value from the ITU grid, optimization of the athermal waveguide for the CAWG router for super PON is necessary with an emphasis on reducing its chromatic dispersion in all four super PON bands.

Authorized licensed use limited to: CVTI - Centre of Scientific and Technical Info. Downloaded on July 21,2026 at 08:11:17 UTC from IEEE Xplore. Restrictions apply.

IV. Conclusion

This paper presented a comprehensive simulation-based analysis of the thermal and chromatic dispersion behavior of a 20-channel, 100 GHz athermal cyclic AWG designed for Super PON applications. The CAWG was implemented using a SiO_xN_y core and PMMA cladding on a silicon substrate with a thermal SiO_2 buffer layer, forming an athermal waveguide structure optimized for minimal temperature-induced central wavelength shifts.

Beyond the thermal optimization, the study introduced a detailed investigation of both waveguide and material dispersion across four spectral bands (C1, C2, L2, and L1). Our results demonstrate that the central wavelength shift of the CAWG in the base C1 band is effectively minimized to 0.2 pm/°C, confirming the success of the athermal design. However, in the other three bands, chromatic dispersion particularly material dispersion becomes increasingly dominant, with the CW offset from the ITU grid reaching up to 0.632 nm in the L1 band.

These findings highlight the importance of considering both waveguide and material dispersion in the design of cyclic AWG structures, especially when targeting broadband applications across multiple spectral periods of cyclic AWG. To ensure compliance with ITU DWDM grid specifications in all Super PON bands, further refinement of the waveguide geometry and material composition is necessary. The presented dual-layered dispersion analysis provides valuable insights for the development of thermally robust and spectrally precise wavelength routing components in next-generation optical access networks based on WDM-TDM PON architectures.

References

[1] D. Seyringer: Arrayed waveguide gratings, SPIE Spotlights, Volume: SL16, Bellingham, Wash., 2016, ISBN 978-1-5106-0359-2

[2] Chovan, J., Kuzma, A., Tomaška, M., & Uherek, F. (2025, September). Optimization of rib, single mode SiOxNy optical waveguide structure for athermal AWG using PMMA cover layer. In Photonics, Devices, and Systems IX (Vol. 13698, p. 1369802). SPIE.

[3] C. DeSanti, L. Du, J. Guarin, J. Bone and C. F. Lam, "Super-PON: an evolution for access networks [Invited]," in Journal of Optical Communications and Networking, vol. 12, no. 10, pp. D66-D77, October 2020, doi: 10.1364/JOCN.391846.

[4] Xiang Wang, Simiao Xiao, Weiwei Zheng, Fan Wang, Yubo Li, Yinlei Hao, Xiaoqing Jiang, Minghua Wang, Jianyi Yang, Athermal silicon arrayed waveguide grating with polymer-filled slot structure, Optics Communications, Volume 282, Issue 14, 2009, Pages 2841-2844, ISSN 0030-4018, https://doi.org/10.1016/j.optcom.2009.04.020

[5] R. Jia, H. Wu, X. Xu, L. Du and J. Zhao, "Athermal Polymer Arrayed Waveguide Grating Router for Optical Backplane," in IEEE Photonics Journal, vol. 17, no. 5, pp. 1-7, Oct. 2025, Art no. 6602107, doi: 10.1109/JPHOT.2025.3605942.

[6] Li, D., et al. "Design of athermal arrayed waveguide grating using silica/polymer hybrid materials." Optica Applicata 37.3 (2007): 305.

[7] Lianghong Yin and Ming Lu and Leszek Wielunski and Weiwei Song and Jun Tan and Yicheng Lu and Wei Jiang; Fabrication and characterization of compact silicon oxynitride waveguides on silicon chips, Journal of Optics, 2012, 14 085501,

[8] A. Trenti, M. Borghi, S. Biasi, M. Ghulinyan, F. Ramiro-Manzano, G. Pucker, L. Pavesi; Thermo-optic coefficient and nonlinear refractive index of silicon oxynitride waveguides. AIP Advances 1 February 2018; 8 (2): 025311. https://doi.org/10.1063/1.5018016.

[9] G. Beadie, M. Brindza, R. A. Flynn, A. Rosenberg, J. S. Shirk. Refractive index measurements of poly(methyl methacrylate) (PMMA) from 0.4-1.6 μm. Appl. Opt. 54, F139-F143 (2015)

[10] G.694.1 : Spectral grids for WDM applications: DWDM frequency grid https://www.itu.int/rec/T-REC-G.694.1-202010-I/en

Authorized licensed use limited to: CVTI - Centre of Scientific and Technical Info. Downloaded on July 21,2026 at 08:11:17 UTC from IEEE Xplore. Restrictions apply.